DOI 10.1007/s11106-019-00055-2
Powder Metallurgy and Metal Ceramics, Vol. 58, Nos. 3-4, July, 2019 (Russian Original Vol. 58, Nos. 3-4, March-April, 2019)

THEORY, MANUFACTURING TECHNOLOGY, AND PROPERTIES OF POWDERS AND FIBERS

PHYSICOCHEMICAL PROPERTIES OF HYDROTHERMAL NANOCRYSTALLINE ZrO_2–Y_2O_3–CeO_2 POWDERS

I.O. Marek,[1,3] O.K. Ruban,[1] V.P. Redko,[1] M.I. Danilenko,[1] S.A. Korniy,[2] and O.V. Dudnik[1]

UDC 541.1:621.762

Nanocrystalline powders in the ZrO_2–Y_2O_3–CeO_2 system were produced by hydrothermal synthesis in an alkaline environment. The powder properties were studied by differential thermal analysis, X-ray diffraction, electron microscopy, petrography, and BET. A low-temperature ZrO_2-based cubic solid solution crystallized in the powders in hydrothermal conditions. The specific surface area of the powders was 81–110 m^2/g. The lattice parameters of the ZrO_2-based solid solution increased monotonically with higher CeO_2 amount. The research results are needed for the microstructural design of composites in the ZrO_2–Y_2O_3–CeO_2 system with high resistance to low-temperature ageing.

Keywords: *ZrO_2–Y_2O_3–CeO_2, ZrO_2-based solid solution, hydrothermal synthesis, nanocrystalline powder, F-ZrO_2.*

INTRODUCTION

Zirconia-based composites in the ZrO_2–Y_2O_3–CeO_2 system are promising for the development of structural, functional, and biomedical materials since they exhibit high strength characteristics and their properties do not degrade at low temperatures in a humid environment. In particular, the constitution of structural and biomedical composites has to correspond to the region in which T-ZrO_2 (tetragonal ZrO_2-based solid solution) exists in the ZrO_2–Y_2O_3–CeO_2 phase diagram to promote effective transformation hardening. There is a direct relationship between the processes for producing the starting powders and the properties of resultant transformation-hardened ZrO_2-based materials [1, 2].

To produce nanocrystalline ZrO_2-based powders, a number of techniques are currently employed. One of them is hydrothermal synthesis (HTS), which combines the advantages of sol–gel process and coprecipitation. The potential to control the nucleation and particle growth processes in hydrothermal synthesis (through change in concentration, decrease or increase in hydrolysis temperature, increase in hydrolysis time, introduction of surfactants during dehydration, change in pH during removal of impurities, etc.) allows high-purity homogeneous powders of

[1]Frantsevich Institute for Problems of Materials Science, National Academy of Sciences of Ukraine, Kyiv, Ukraine. [2]Karpenko Physicomechanical Institute, National Academy of Sciences of Ukraine, Lviv, Ukraine.

[3]To whom correspondence should be addressed; e-mail: Mega_marekirina@ukr.net.

Translated from Poroshkova Metallurgiya, Vol. 58, Nos. 3–4 (526), pp. 3–12, 2019. Original article submitted October 22, 2018.

different shapes to be produced in these conditions. These powders do not require additional grinding or heat treatment operations at high temperatures that commonly lead to contamination of the powders and decrease their activity in sintering. The properties of 'perfect' and hydrothermally synthesized powders were compared; it was revealed that the hydrothermal powders had properties close to those of 'perfect' nanocrystalline powders [3, 4].

Among the various HTS options to produce nanocrystalline ZrO_2-based powders [5–8], hydrothermal synthesis in acidic [9–11] and alkaline [12–17] environments and HTS combined with mechanical mixing [18] or microwave heating [19, 20] have been recently employed. Hydrothermal synthesis is used to deposit coatings [21–23] and make microspheres [24], catalysts [25–29], and functional nanomaterials [30, 31].

Hydrothermal synthesis of nanocrystalline ZrO_2-based powders in an alkaline environment can produce composites of various constitutions and for various purposes [1, 2], including biomedical applications [32]. The ZrO_2-based composites acquired the required mechanical properties at an optimum content of stabilizers: 2–3 mol.% Y_2O_3 and 8–12 mol.% CeO_2 [12]. These findings underlay the choice of compositions for nanocrystalline powders in the ZrO_2–Y_2O_3–CeO_2 system to be studied, wt.%: $97ZrO_2$–$3Y_2O_3$ → Zr(3Y), $95ZrO_2$–$3Y_2O_3$–$2CeO_2$ → Zr(3Y2Ce), $92.5ZrO_2$–$2.5Y_2O_3$–$5CeO_2$ → Zr(2.5Y5Ce), $90ZrO_2$–$2Y_2O_3$–$8CeO_2$ → Zr(2Y8Ce), and $88ZrO_2$– $12CeO_2$ → Zr(12Ce).

The objective of this paper is to examine the properties of ZrO_2-based solid-solution powders produced by hydrothermal synthesis in an alkaline environment.

The knowledge of these properties is a prerequisite for the microstructural design of advanced ZrO_2-based composites in the ZrO_2–Y_2O_3–CeO_2 system, whose properties would not degrade at low temperatures in a humid environment. The microstructural design of ZrO_2–Y_2O_3–CeO_2 composites relies on a four-term relationship of physicochemical analysis, such as 'composition → structure → particle size → properties', establishing links between all stages of producing these composites [1]. The use of dispersions for developing ZrO_2-based materials raises inevitable questions about their activity and metastability since the presence of metastable phases besides equilibrium ones may significantly influence the microstructural design of the composites.

EXPERIMENTAL PROCEDURE

The production of nanocrystalline powders in the ZrO_2–Y_2O_3–CeO_2 system by hydrothermal synthesis in an alkaline environment is described in detail in our paper [33]. The main distinction of the synthesis procedure employed in this research effort is that zirconium oxychloride ($ZrOCl_2 \cdot 8H_2O$), yttrium nitrate ($Y(NO_3)_3 \cdot 6H_2O$), and cerium nitrate ($Ce(NO_3)_3 \cdot 6H_2O$) were chosen as the starting components instead of zirconium oxynitrate ($ZrO(NO_3)_2 \cdot 8H_2O$). The hydrothermal synthesis used only water that remained in coprecipitated hydroxides of the starting components after boiling and filtering. The hydrothermal treatment to synthesize nanocrystalline powders in an alkaline environment was conducted using a laboratory autoclave at 225°C for 4 h (1.6 MPa pressure in the autoclave corresponded to the saturated water vapor pressure at this temperature). Following the hydrothermal synthesis, a mother solution formed above the precipitate and the precipitate volume became ~25–30% smaller compared to the starting mixtures. The powders were dried at 60°C for 8 h.

The powders' properties were examined by X-ray diffraction (DRON-1.5, Cu-K_α radiation source, scanning rate 1–4°/min, $2\theta = 15$–90°), differential thermal analysis (DTA) (Q-1500 D derivatograph, 10°C/min heating rate in range 20–1000°C), electron microscopy (JEM-2100 F and ZEISS EVO 40 XVP microscopes), and electron microprobe analysis (Philips Analytical X-ray diffractometer). The sizes of primary particles were determined with the Scherrer equation. The petrographic method was used for microstructural analysis with a MIN-8 microscope and a standard set of immersion liquids (60–620 magnification). The specific surface area of the nanocrystalline powders was measured by thermal nitrogen adsorption (BET).

RESULTS AND DISCUSSION

Electron microprobe analysis showed that the compositions of Zr(3Y), Zr(3Y2Ce), Zr(2.5Y5Ce), Zr(2Y8Ce), and Zr(12Ce) powders synthesized hydrothermally in an alkaline environment corresponded to those

calculated previously, and the integral content of CaO, HfO_2, La_2O_3, and Nd_2O_3 admixtures was no more than 1 wt.%.

Figure 1 presents DTA curves from powder derivatograms. All DTA curves show intensive endothermic effects with minima at 100–110°C, associated with the removal of adsorbed water from the powders. The most intensive effect is seen on the DTA curve for the Zr(2Y8Ce) powder. Note that these processes were accompanied by a 5 to 6% weight loss of the Zr(3Y), Zr(3Y2Ce), Zr(2.5Y5Ce), and Zr(12Ce) powders and by a 9% weight loss of the Zr(2Y8Ce) powder. The minor endothermic effects on the DTA curves observed at 220–230°C for all compositions are also associated with the removal of residual water. Contrastingly, they were not accompanied by significant weight losses. The DTA curves show sharp exothermic effects for the Zr(12Ce), Zr(2Y8Ce), and Zr(3Y2Ce) powders at 310–320°C and a flattened exothermic effect for the Zr(2.5Y5Ce) powder at the same temperatures. We assume that these effects are associated with the crystallization of the amorphous phase that remained after HTS in an alkaline environment.

Differential thermal analysis established the total weight loss of the samples, %: 9 for Zr(3Y), 9 for Zr(3Y2Ce), 10 for Zr(2.5Y5Ce), 12 for Zr(2Y8Ce), and 11 for Zr(12Ce). This weight loss of the samples when heated to 500°C is due to the loss of structural (bound) water that remained in the powders after HTS.

Figure 2 presents X-ray diffraction patterns for the powders synthesized hydrothermally in an alkaline environment, and Table 1 summarizes their phase compositions. It is seen (Fig. 2) that thermodynamically nonequilibrium systems formed in the powders, which include a low-temperature metastable cubic ZrO_2-based (F-ZrO_2) solid solution. Note also that the F-ZrO_2 lattice parameters increase with higher CeO_2 content of the ZrO_2-based solid solution (Table 1).

The formation of metastable low-temperature F-ZrO_2 when the Zr(3Y), Zr(3Y2Ce), Zr(2.5Y5Ce), Zr(2Y8Ce), and Zr(12Ce) powders crystallize in hydrothermal conditions is an expected process that obeys Ostwald's step rule and Dankov's orientation–dimensional principle [34–36]. Under pressure of saturated water vapors, the nanocrystalline powders of ZrO_2-based solid solutions form both through 'topotactic crystallization' of F-ZrO_2 on nuclei in amorphous ZrO_2 gel and through dissolution–crystallization. The topotactic crystallization mechanism complies with Ostwald's step rule. According to this rule, a compound that exists in several polymorphic modifications crystallizes in steps: the unstable modification with higher Gibbs energy shows up first and then, in appropriate conditions, transforms to the stable modification with the minimum Gibbs energy. Hence, when a substance has more than one modification, the least stable modification crystallizes first and then finally transforms to the most stable one.

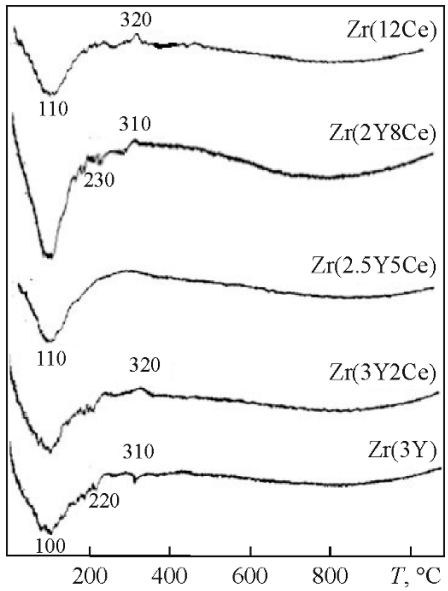

Fig. 1. DTA curves for hydrothermally synthesized nanocrystalline powders in the ZrO_2–Y_2O_3–CeO_2 system

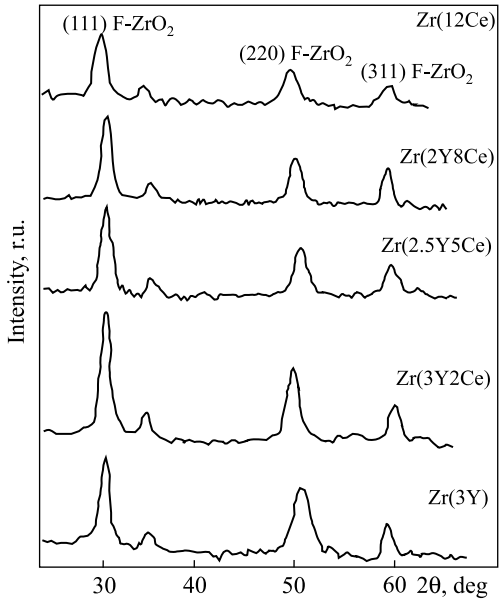

Fig. 2. X-ray diffraction patterns for hydrothermally synthesized nanocrystalline powders in the ZrO_2–Y_2O_3–CeO_2 system

TABLE 1. Physicochemical Properties of Powders in the ZrO_2–Y_2O_3–CeO_2 System

Powder	Phase composition	Specific surface area, m^2/g	Particle size, nm	Lattice parameters	
				a_f, nm	V_f, nm^3
Zr(3Y)	F-ZrO_2	99	6/10*	0.5126	0.1347
Zr(3Y2Ce)	F-ZrO_2	81	7/12	0.5143	0.1361
Zr(2.5Y5Ce)	F-ZrO_2	110	8/9	0.5157	0.1371
Zr(2Y8Ce)	F-ZrO_2	93	9/10	0.5159	0.1373
Zr(12Ce)	F-ZrO_2	106	7/9	0.5161	0.1375

*According to Scherrer's equation/specific surface area.

A mixture of coprecipitated hydroxides is a thermodynamically unstable system that, in compliance with Ostwald's rule, transforms directly to metastable F-ZrO_2. Hydrothermal treatment leads to the formation of zirconium hydroxocomplex, $[Zr(OH)_2 \cdot 4H_2O]_4^{8+} \cdot (OH)_8^{-}]$, with a near-cubic structure. For this reason, the crystallization of metastable F-ZrO_2 obeys also Dankov's orientation principle: phase transformations on a solid proceed in the direction of a new crystalline lattice whose orientation and dimensions correspond to the crystalline lattice of the starting surface [34]. Therefore, low-temperature metastable F-ZrO_2 forms when the Zr(3Y), Zr(3Y2Ce), Zr(2.5Y5Ce), Zr(2Y8Ce), and Zr(12Ce) nanosized powders crystallize at the highest rate since its structure is the least different from that of the starting mixture of coprecipitated oxides.

The powders' specific surface area (Table 1) falls into the range 81–110 m^2/g. Noteworthy is that there is no direct correlation between the specific surface areas of the Zr(3Y), Zr(3Y2Ce), Zr(2.5Y5Ce), Zr(2Y8Ce), and Zr(12Ce) powders and CeO_2 content of the ZrO_2-based solid solution. Table 1 also shows sizes of primary particles in the powders of all compositions calculated with Scherrer's equation and data on the specific surface areas. The values agree with each other.

According to microstructural analysis carried out with the petrographic method employing an optical microscope, areas with different crystal optical characteristics formed in the powders: crystalline areas containing

high-relief particles (F-ZrO_2) and transparent ones. The high-relief particles are due, in particular, to a great difference between the refractive indices of ZrO_2 and the experimental liquid agent. The fact that all powders are isotropic and agglomerates are not polarized confirms that low-temperature metastable F-ZrO_2 forms in the Zr(3Y), Zr(3Y2Ce), Zr(2.5Y5Ce), Zr(2Y8Ce), and Zr(12Ce) powders.

At the same time, the ratio of crystalline and amorphous areas changes in the powders. The Zr(3Y) powder contains only individual transparent isotropic areas, while the number of transparent isotropic areas in the Zr(3Y2Ce) powder increases to ~10%.

It should be noted that F-ZrO_2 crystallizes at the boundaries of these areas. The Zr(2.5Y5Ce) powder contains ~25% of transparent isotropic agglomerates with layers of crystalline F-ZrO_2 particles being formed at their boundaries. The Zr(2Y8Ce) powder already contains transparent areas with layered rims of a crystalline phase with high-relief particles (F-ZrO_2) at its boundaries. The crystal optical characteristics of the Zr(12Ce) powder are similar to those peculiar to the Zr(2Y8Ce) powder. Microstructural analysis shows that the amount of the isotropic phase with a layered rim of the crystalline phase with high-relief particles (F-ZrO_2) decreases with a greater amount of cerium oxide in the ZrO_2-based solid solution. In addition, the experiments confirmed the conclusion of differential thermal analysis: exothermic peaks on DTA curves for the Zr(3Y), Zr(3Y2Ce), Zr(2.5Y5Ce), Zr(2Y8Ce), and Zr(12Ce) powders (Fig. 1) are associated with the crystallization of the amorphous phase that remained in the powders synthesized hydrothermally in an alkaline environment.

Morphological analysis carried out by electron microscopy revealed a three-layer structure in the powders: primary particles–aggregates–agglomerates. The morphology of primary particles is presented in Fig. 3*a*. This microphotograph is typical of all powders studied. Round primary particles ~5 nm in size were revealed. The results confirm the calculated sizes of primary powder particles (Table 1). Clear separation of the lattices is seen (Fig. 3*a*). This testifies that the ZrO_2-based solid solutions crystallize in the Zr(3Y), Zr(3Y2Ce), Zr(2.5Y5Ce), Zr(2Y8Ce), and Zr(12Ce) nanosized powders in the hydrothermal synthesis process. The morphology of primary particle aggregates is presented in Fig. 3*b–f*. Weak aggregates of primary particles are seen.

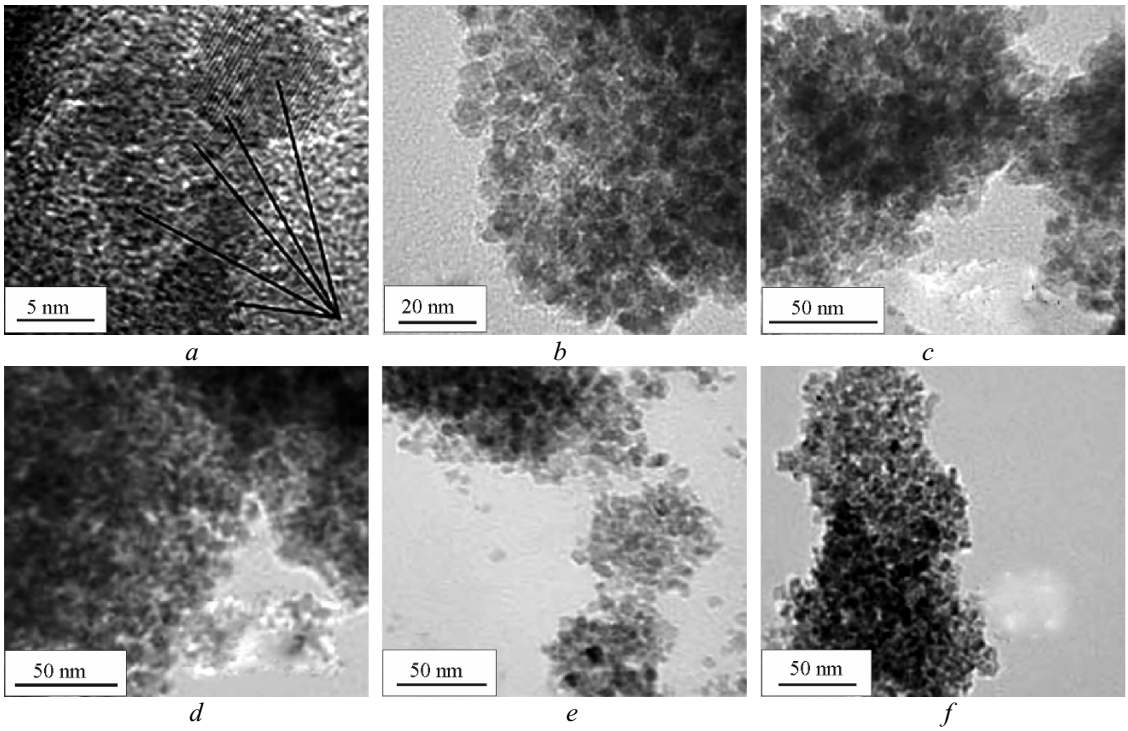

Fig. 3. Morphology of primary particles (*a*) and particle aggregates (*b–f*) in hydrothermally synthesized powders in the ZrO_2–Y_2O_3–CeO_2 system: *b*) Zr(3Y); *c*) Zr(3Y2Ce); *d*) Zr(2.5Y5Ce); *e*) Zr(2Y8Ce); *f*) Zr(12Ce)

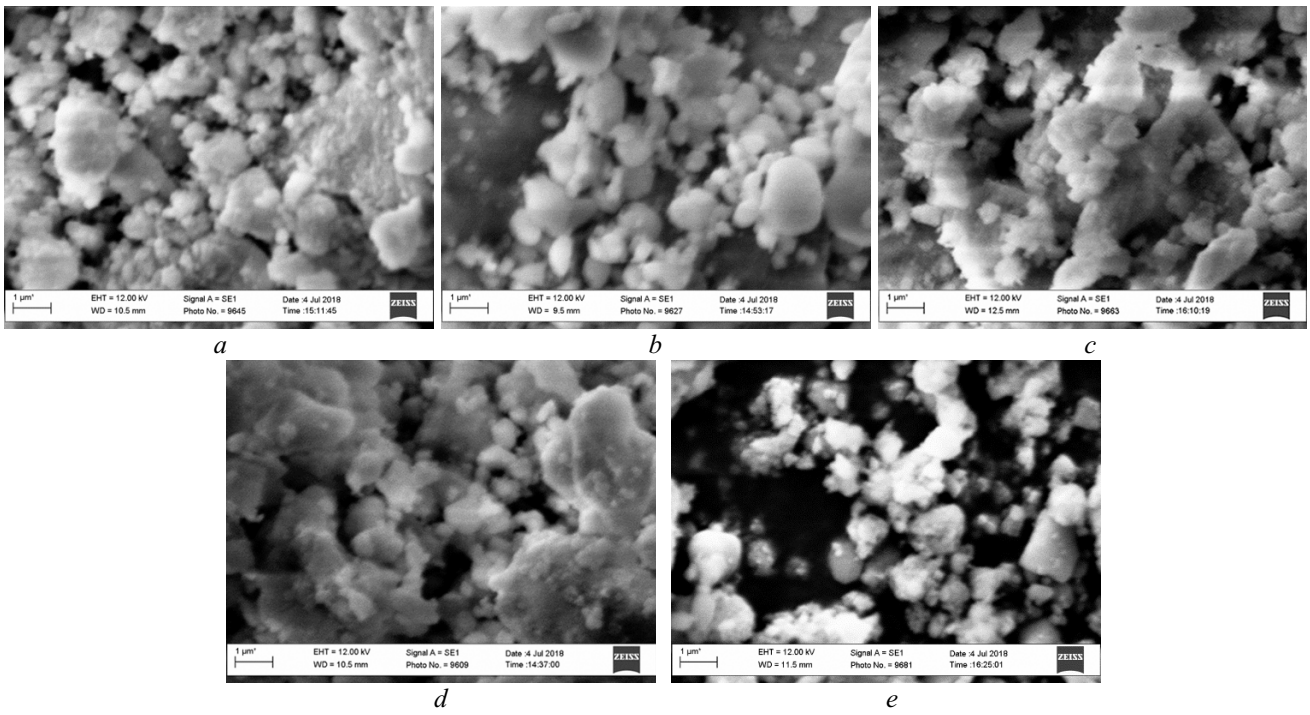

Fig. 4. Morphology of agglomerates in hydrothermally synthesized powders in the ZrO_2–Y_2O_3–CeO_2 system: *a*) Zr(3Y); *b*) Zr(3Y2Ce); *c*) Zr(2.5Y5Ce); *d*) Zr(2Y8Ce); *e*) Zr(12Ce)

The morphology of powder agglomerates is shown in Fig. 4. 'Soft' round agglomerates from 0.2–0.5 to 5 μm in size formed in the powders; they easily failed in microstructural experiments. With higher CeO_2 content of the ZrO_2-based solid solution, the agglomerates decreased in size: the average size of the Zr(12Ce) powder agglomerates is half as great as that of the Zr(3Y) agglomerates.

CONCLUSIONS

A low-temperature metastable cubic ZrO_2-based solid solution (F-ZrO_2) crystallizes in the Zr(3Y), Zr(3Y2Ce), Zr(2.5Y5Ce), Zr(2Y8Ce), and Zr(12Ce) powders in hydrothermal conditions. The lattice parameters of the ZrO_2-based solid solution increase with higher CeO_2 content. In addition, higher CeO_2 content of the powders decreases the amount of the residual amorphous phase that crystallizes when the powders are further heat-treated.

There is no direct correlation between the specific surface area of the nanocrystalline powders and CeO_2 content of the ZrO_2-based solid solution. The nanocrystalline powders generally show a three-layer structure: primary particles (~5–10 nm)–aggregates–agglomerates. The formation of low-temperature metastable F-ZrO_2 leads to nonequilibrium resultant powders that are highly active in the production of ZrO_2–Y_2O_3–CeO_2 composites.

The use of respective approaches to heat treatment and consolidation processes for the microstructural design of composites from the Zr(3Y), Zr(3Y2Ce), Zr(2.5Y5Ce), Zr(2Y8Ce), and Zr(12Ce) powders will allow the production of advanced ceramic materials whose properties would not degrade at low temperatures in a humid environment.

ACKNOWLEDGMENTS

The authors are grateful to V.M. Pavlikov, PhD in Chemical Sciences, for the differential thermal analysis and to L.D. Bilash for determining the powders' specific surface area.

REFERENCES

1. E.V. Dudnik, A.V. Shevchenko, A.K. Ruban, V.P. Red'ko, and L.M. Lopato, "Microstructural design of ZrO_2–Y_2O_3–CeO_2–Al_2O_3 materials," *Powder Metall. Met. Ceram.*, **49**, Nos. 9–10, 528–536 (2011).
2. E.V. Dudnik, S.N. Lakiza, Ya.S. Tishchenko, A.K. Ruban, V.P. Red'ko, A.V. Shevchenko, and L.M. Lopato, "Phase diagrams of refractory oxide systems and microstructural design of materials," *Powder Metall. Met. Ceram*., **53**, Nos. 5–6, 303–311 (2014).
3. S. Sōmiya and T. Akiba, "Hydrothermal zirconia powders: A Bibliography," *J. Eur. Ceram. Soc*., **19**, No. 1, 81–87 (1999).
4. A.V. Shevchenko, "Hydrothermal techniques in materials science," in: *Inorganic Materials Science. Fundamentals of Materials Science* [in Russian], Kyiv (2008), Vol. 2, pp. 272–281.
5. O. Vasylkiv and Y. Sakka, "Hydroxide synthesis, colloidal processing and sintering of nano-size 3Y-TZP powder," *Scripta Mater.*, **44**, 2219–2223 (2001).
6. O. Vasylkiv, Y. Sakka, and V. Skorokhod, "Low-temperature processing and mechanical properties of zirconia and zirconia-alumina nano-ceramic," *J. Am. Ceram. Soc*., **86**, No. 2, 299–304 (2003).
7. O. Vasylkiv and Y. Sakka, "Synthesis and colloidal processing of zirconia nano-powder," *J. Am. Ceram. Soc*., **84**, No. 11, 2489–2494 (2001).
8. E.V. Dudnik, "Modern methods for hydrothermal synthesis of ZrO_2-based nanocrystalline powders," *Powder Metall. Met. Ceram*., **48**, Nos. 3–4, 238–248 (2009).
9. Z. Yanjie, Z. Yingying, C. Yanning, C. Chongqi, L. Xingyi, and Z. Qi, "Low-temperature water–gas shift reaction over Au/ZrO_2 catalysts using hydrothermally synthesized zirconia as supports," *Chin. J. Catal.*, **33**, 230–236 (2012).
10. Yu.M. Fedenko, T.A. Dontsova, and I.M. Astrelin, "Turbidimetric method for estimating the sizes of nanoparticles in ZrO_2 white sols," *Nauk. Vist. NTUU KPI*, Issue 1, 155–158 (2012).
11. M. Taguchi, T. Nakane, A. Matsushita, Y. Sakka, T. Uchikoshi, T. Funazukuri, and T. Naka, "One-pot synthesis of monoclinic ZrO_2 nanocrystals under subcritical hydrothermal conditions," *J. Supercrit. Fluids*, **85**, 57–61 (2014).
12. E.V. Dudnik and A.V. Shevchenko, "Variation in properties of ZrO_2–Y_2O_3–CeO_2–Al_2O_3 powders during thermal treatment at 400 to 1300°C," *Powder Metall. Met. Ceram*., **49**, Nos. 3–4, 125–134 (2010).
13. A. Behbahani, S. Rowshanzamir, and A. Esmaeilifar, "Hydrothermal synthesis of zirconia nanoparticles from commercial zirconia," *Procedia Eng.*, **42**, 908–917 (2012).
14. L.M. Rudkovskaya, R.N. Pshenichny, T.V. Pavlenko, and A.A. Omelchuk, "Nanostructured zirconium dioxide synthesized hydrothermally from zirconium concentrate decomposition products," *Nanosyst. Nanomater. Nanotekhnol.*, **10**, No. 2, 351–360 (2012).
15. R. Espinoza-Gonzáleza, E. Mosquera, I. Moglia, R. Villarroel, and V.M. Fuenzalida, "Hydrothermal growth and characterization of zirconia nanostructures on non-stoichiometric zirconium oxide," *Ceram. Int.* (2014), URL: [http://dx.doi.org/10.1016/ j.ceramint.2014.07.034].
16. Ch.V. Reddy, I.N. Reddy, J. Shim, D. Kim, and K. Yoo, "Synthesis and structural, optical, photocatalytic, and electrochemical properties of undoped and yttrium-doped tetragonal ZrO_2 nanoparticles," *Ceram. Int.* (2018), URL: [https://doi.org/10.1016/j.ceramint.2018.04.020].
17. G. Growth, L. Fei, L. Yanhuai, S. Zhongxiao, X. Kewei, M. Dayan, G. Bo, and C. Hon, "Characteristics of hydrothermally prepared yttria stabilized zirconia nanocrystals during calcination," *Rare Met. Mater. Eng.*, **46**, No. 4, 899–905 (2017).
18. C. Duran, K. Sato, Y. Hotta, H. Göçmez, and K. Watari, "Ball milling assisted hydrothermal synthesis of ZrO_2 nanopowders," *Ceram. Int.*, **41**, 5588–5593 (2015).
19. A.O. Hongmin, L.U. Xiangsheng, Z. He, Z. Jing, H. Xiaowei, F. Zongyu, and X. Hong, "Preparation of scandia stabilized zirconia powder using microwave-hydrothermal method," *J. Rare Earths*, **33**, No. 7, 746–751 (2015).

20. J. Liao, Q. Wang, L. Nie, W. You, and J. Chen, "Single red upconversion and near-infrared downconversion luminescence properties of cubic ZrO_2:Y^{3+}–Yb^{3+}–Er^{3+} nanophosphors via microwave hydrothermal synthesis," *Opt. Mater.*, **62**, 479–484 (2016).
21. M. Asiltürk, E. Burunkaya, F. Sayilkan, N. Kiraz, and E. Arpaç, "Structural and optical properties of thin films prepared from surface modified ZrO_2," *J. Non-Cryst. Solids*, **357**, 206–210 (2011).
22. X. Gan, Z. Yu, K. Yuan, C. Xu, X. Wang, L. Zhu, G. Zhang, and D. Xu, "Preparation of a CeO_2-nanoparticle thermal radiation shield coating on ZrO_2 fibers via a hydrothermal method," *Ceram. Int.* (2017), URL: [http://dx.doi.org/10.1016/j.ceramint.2017.07.161. 2017].
23. L.J. Zhao, W. Zai, M.H. Wong, and H.C. Man, "Hydrothermal synthesis of Ag-ZrO_2/*r*-GO coating on CoCrMo substrate," *Mater. Lett.*, **228**, 314–317 (2018).
24. Zh. Song, C. Duan, M. Shi, S. Li, and Y. Guan, "One-step preparation of ZrO_2/SiO_2 microspheres and modification with *d*-fructose 1, 6-bisphosphate as stationary phase for hydrophilicinteraction chromatography," *J. Chromatogr*. (2017), URL: [http://dx.doi.org/10.1016/ j.chroma.2017.09.046].
25. O. Vasylkiv, Y. Sakka, Y. Maeda, and V.V. Skorokhod, "Nano-engineering of zirconia-noble metals composites," *J. Eur. Ceram. Soc.*, **24**, No. 2, 469–473 (2004).
26. O. Vasylkiv, Y. Sakka, Y. Maeda, and V.V. Skorokhod, "Sonochemical preparation and properties of Pt–3Y-TZP nano-composites," *J. Am. Ceram. Soc.*, **88**, No. 3, 639–644 (2005).
27. O.V. Almiasheva, A.Yu. Postnov, N.V. Maltseva, and E.A. Vlasov, "Thermally stable catalyst based on ZrO_2–Al_2O_3 nanocomposite for hydrogen oxidation," *Nanosyst. Fiz. Khim. Mat.*, **3**, No. 6, 75–82 (2012).
28. Zh. Song, P. Ning, Q. Zhang, H. Li, J. Zhang, Y. Wang, X. Liu, and Z. Huang, "Activity and hydrothermal stability of CeO_2–ZrO_2–WO_3 for the selective catalytic reduction of NO_x with NH_3," *J. Environ. Sci.* (2015), URL: [http://dx.doi.org/10.1016/j.jes.2015.06.010].
29. P. Ning, Z. Song, H.Li, Q. Zhang, X. Liu, J. Zhang, X. Tang, and Z. Huang, "Selective catalytic reduction of NO with NH_3 over CeO_2–ZrO_2–WO_3 catalysts prepared by different methods," *Appl. Surf. Sci*. (2015), URL: [http://dx.doi.org/10.1016/j.apsusc.2015.01.118].
30. A.I. Ramos-Guerra, I. Martínez-Merlín, and C. Falcony, "The role of the stabilizing agent on the structural and luminescent properties of hydrothermally synthesized ZrO_2: Tb^{3+}phosphors," *Ceram. Int.* (2018), URL: [https://doi.org/10.1016/j.ceramint.2018.04.216].
31. M.A.I. Mohamed, V.-D. Dao, S.Y. Ahmed, M.M. Hamouda, A.Y. Mohamed, Y.K. Muhammad, H.-S. Choi, and A.M.B. Nasser, "Physicochemical and photo-electrochemical characterization of novel N-doped nanocomposite ZrO_2/TiO_2 photoanode towards technology of dye-sensitized solar cells," *Mater. Charact.* (2017), URL: [doi: 10.1016/j.matchar.2017.03.014].
32. A.V. Shevchenko, E.V. Dudnik, V.V. Tsukrenko, A.K. Ruban, V.P. Red'ko, and L.M. Lopato, "Microstructural design of bioinert composites in the ZrO_2–Y_2O_3–CeO_2–Al_2O_3–CoC system," *Powder Metall. Met. Ceram*., **51**, Nos. 11–12, 724–733 (2012).
33. A.V. Shevchenko, E.V. Dudnik, A.K. Ruban, V.M. Vereschaka, V.P. Red'ko, and L.M. Lopato, "Hydrothermal synthesis of nanocrystalline powders in the ZrO_2−Y_2O_3−CeO_2 system," *Powder Metall. Met. Ceram*., **46**, Nos. 1–2, 18–24 (2007).
34. I.M. Vasserman, *Chemical Solution Deposition* [in Russian], Leningrad (1980), p. 208.
35. O.Yu. Kurapova, V.G. Konakov, S.N. Golubev, and V.M. Ushakov, "Interaction between the synthesis procedure, phase formation, and particle size of precursor powders for ceramics with final composition 9CaO91ZrO_2," *Nov. Ogneupory*, No. 4, 47–52 (2014).
36. O.Yu. Kurapova, V.G. Konakov, S.N. Golubev, and V.M. Ushakov, "Phase formation and stability of solid solutions in nanosized zirconia dioxide precursors produced by cryochemical methods," *Vest. SPb Gos. Univ. Ser. 4: Fiz. Khim.*, **3(61)**, 296–310 (2016).